Article

Engineering NiS/Ni2P Heterostructures for Efficient Electrocatalytic Water Splitting

Xin Xiao, Dekang Huang, Yong Qing Richard Fu, Ming Wen, Xingxing Jiang, Xiaowei Lv, Man Li, Lin Gao, Shuangshuang Liu, Mingkui Wang, Chuan Zhao, and Yan Shen

ACS Appl. Mater. Interfaces, **Just Accepted Manuscript** • DOI: 10.1021/acsami.7b16430 • Publication Date (Web): 15 Jan 2018

Engineering NiS/Ni_2P Heterostructures for Efficient Electrocatalytic Water Splitting

Xin Xiao,[†] Dekang Huang,[‡] Yong Qing Fu,[⊥] Ming Wen,[§] Xingxing Jiang,[†] Xiaowei Lv,[†] Man Li,[†] Lin Gao,[†] Shuangshuang Liu,[†] Mingkui Wang,[†] Chuan Zhao,[#] Yan Shen,[†]*

[†] Wuhan National Laboratory for Optoelectronics, Huazhong University of Science and Technology, Wuhan 430074, P. R. China

[‡] College of Science, Huazhong Agricultural University, Wuhan 430070, P. R. China

[⊥] Faculty of Engineering and Environment, Northumbria University, Newcastle Upon Tyne, NE1 8ST, UK

[§] School of Chemistry Science and Engineering, Tongji University, Shanghai 200092, P. R. China

[#] School of Chemistry, The University of New South Wales, Sydney, NSW, 2052, Australia

KEYWORDS: Bifunctional electrocatalyst, heterostructures, nickel phosphide, nickel sulfide, overall water splitting

ABSTRACT

Developing high-active and low-cost bifunctional materials for catalyzing hydrogen evolution reaction (HER) and oxygen evolution reaction (OER) holds pivotal role in water splitting. Therefore, we present a new strategy to form NiS/Ni_2P heterostructures. The as-obtained NiS/Ni_2P/CC requires overpotentials of 111 mV for the HER and 265 mV for the OER to reach a current density of 20 mA cm^{-2}, outperforming their counterparts such as NiS and Ni_2P under the same conditions. Additionally, the NiS/Ni_2P/CC electrode requires a 1.67 V cell voltage to deliver 10 mA cm^{-2} in two-electrode electrolysis system, which is comparable to the cell using the benchmark Pt/C||RuO_2 electrode. Detailed characterizations reveal that strong electronic interactions between NiS and Ni_2P, abundant active sites, and smaller charge transfer resistance contribute to the improved HER and OER activity.

1. INTRODUCTION

The development of renewable fuels to replace traditional fossil fuels is highly demanded for addressing the increasingly serious energy and environmental issues facing the society.[1] Hydrogen generated from water splitting provides a very promising strategy for the above-mentioned issues because hydrogen can act as an energy carrier and the combustion product is only water.[2] However, the hydrogen production *via* water splitting faces the problem of high energy consumption associated with the high electrolysis potential.[3] RuO_2 and Pt-based materials are commonly considered to be the best electrocatalysts for oxygen evolution reaction (OER) and hydrogen evolution reaction (HER), respectively.[4-7] However, the scarcity of these precious metal electrocatalysts inevitably hinders their large-scale applications.

Over the past few decades, separated non-noble metal catalysts that are optimized for HER and OER have emerged as novel materials for catalyzing water splitting, such as transition metal nitrides[8,9], carbides[10,11] and sulfides[12] for HER, perovskite oxides,[13,14] transition metal oxides[15,16] and hydroxides[17,18] for OER, which are quite prospective to replace precious metal catalysts in large-scale applications. However, developing efficient and durable bifunctional electrocatalysts toward both HER and OER in the same electrolytes with advantages in terms of not only simplifying system and reducing costs, but also providing high efficiency are quite challenge.[19-21]

Recently, earth-abundant transition metal compounds have been corroborated to show decent electrochemical activity and exhibit high durability for both HER and OER, which is quite suitable for their application in water splitting.[22-23] In spite of this, the activity of those reported bifunctional catalysts for catalyzing water splitting reaction are still inferior to that of Pt||RuO_2 couple. Therefore, much efforts have been paid to promote catalytic performance of electrocatalysts over the past few decades.[24-28] Various strategies have been employed to rationally design catalysts,

including creation of active sites by increasing phase boundaries among different components, promoting H atom adsorption and desorption kinetics on catalysts' surface through adjusting charge distribution among different components, and rationally electrode structure design, etc. For example, Zheng *et al.* realized NiS_2-MoS_2 nanoflake-nanowires heterostructure via interface-engineering, in which MoS_2 nanosheets were highly dispersed inside NiS_2 framework, and the authors attributed the significantly enhanced HER catalytic activity to abundant nano-interfaces and defects.[29] He *et al.* revealed that strong interface interaction and redistribution of electrons between W_xC and WS_2 in the $W_xC@WS_2$ heterostructure play a crucial role for the enhanced HER activity.[30] Furthermore, the growth of catalysts onto a three-dimensional (3D) conductive substrate such as carbon cloth would offer strong adhesion and reduce interfacial impedance, which are all beneficial to promoting the electrochemical activity.

Collectively, above mentioned findings indicate that it's quite reasonable to engineer a novel heterostructures in pursuit of enhanced catalytic activity. Furthermore, Ni-based sulfides and phosphides have been demonstrated to be earth-abundant electrocatalysts for both HER and OER. Herein, we developed a three-step method to fabricate NiS/Ni_2P heterostructure on carbon cloth (denoted as NiS/Ni_2P/CC). The as-obtained NiS/Ni_2P/CC requires overpotentials of 111 mV for the HER and 265 mV for the OER in 1 M KOH solution to reach 20 mA cm^{-2}, outperforming their counterparts such as NiS and Ni_2P under the same conditions. Additionally, the NiS/Ni_2P/CC electrode requires a 1.67 V cell voltage to deliver 10 mA cm^{-2} in two-electrode electrolysis system, which is comparable to the cell using the benchmark Pt/C||RuO_2 electrode.

2. EXPERIMENT SECTION

Material Preparation. Scheme 1 depicts the design and integration of NiS/Ni_2P nanosheet arrays on carbon cloth substrate to realize cost-effective catalyst for HER and OER. The

$Ni(OH)_2$/CC were prepared via hydrothermal reaction similar to that reported in the literature.[31] In a typical synthesis, 4 mmol of nickel nitrate hexahydrate, 20 mmol of urea, and 12 mmol of ammonium fluoride were mixed in 50 mL of deionized water under stirring. The cleaned CC (2.5 × 4 cm^2) was immersed into the above solution and reacted at 120 ℃ for 6 hrs in Teflon-lined stainless steel autoclave. After that, the $Ni(OH)_2$/CC was washed with ethanol and water, and then dried at 60 ℃. The synthesis of NiS/$Ni(OH)_2$/CC was also via a hydrothermal reaction.[31] Typically, 0.1 g of Na_2S was dissolved in 25 mL of water under stirring, and then, the above solution with the prepared $Ni(OH)_2$/CC was reacted at 150 ℃ for 6 hrs in a Teflon-lined stainless steel autoclave. After that, the precursor $Ni(OH)_2$/CC was partially sulfurized and the NiS/$Ni(OH)_2$/CC was obtained. For preparing NiS/Ni_2P/CC, the NiS/$Ni(OH)_2$/CC and 0.1 g of NaH_2PO_2 were put at the downstream and upstream side of the tube furnace, respectively, which is similar to that reported

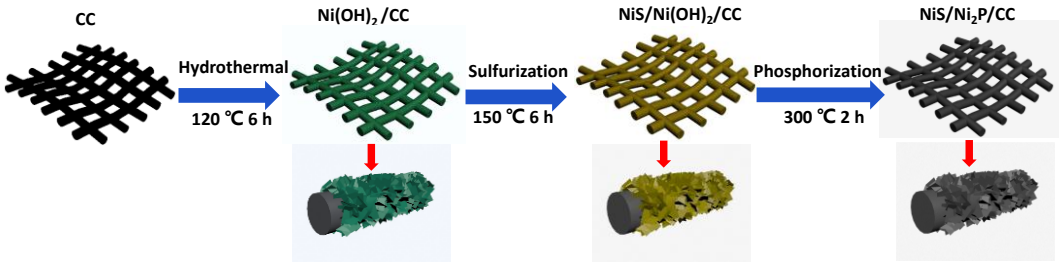

Scheme 1. Schematic illustration of the preparation of NiS/Ni_2P nanosheet arrays on carbon cloth (CC).

in the literature.[32] Subsequently, the NiS/$Ni(OH)_2$/CC was annealed at 300 ℃ for 120 min in N_2 atmosphere to obtain NiS/Ni_2P/CC. The amount of the catalyst supported on the CC was about 5.68 mg cm^{-2}. To obtain NiS/CC, $Ni(OH)_2$/CC was immersed in 25 mL of water with 0.2 g of Na_2S and reacted at 150 ℃ for 6 hrs. To obtain pure Ni_2P/CC, the $Ni(OH)_2$/CC and 0.5 g of NaH_2PO_2 were put in the tube furnace and annealed at 300 ℃ for 120 min in N_2 atmosphere.

Material Characterizations. X-ray diffraction (XRD) tests were conducted on X'pert PRO diffractometer to analyze crystal phases of the as-prepared samples. Scanning electron microscope (SEM) and energy dispersive X-ray spectrometry (EDX) measurements were performed on Nova NanoSEM 450 to characterize the morphology and chemical elements of as-obtained materials, respectively. Transmission electron microscope (TEM) characterization was carried out on FEI Titan 60-300Cs to characterize lattice fringes and chemical elements. X-ray photoelectron spectroscopy (XPS) characterization was conducted on a VG Multilab 2000 XPS instrument to analyze chemical binding states of various ions.

Electrochemical Measurements. Electrochemical tests were performed on a three-electrode electrochemical cell. The presented potentials in this study were all converted to reversible hydrogen electrode (RHE) via the equation: $E_{RHE} = E_{Ag/AgCl} + 1.023$.[33] All the polarization curves were recorded using a linear sweep voltammetry (LSV). Unless specifically mentioned, LSV was recorded with 95% *iR* compensation because the tested curves only showed a slightly fluctuation at this level of compensation. To measure double-layer capacitance (C_{dl}), the cyclic voltammetry measurement with different scan rates ranging from 10 to 100 mV s^{-1} was carried out at the potential windows between 0.3 to 0.5 V vs. RHE. The obtained C_{dl} can be converted into an electrochemical active surface area (ECSA) using the formula: ECSA= $\frac{C_{dl}}{C_s}$, where the specific capacitance value was 40 μF cm^{-2}.[6]

3. RESULTS AND DISCUSSION

SEM image in Figure 1a exhibits that $Ni(OH)_2$ nanosheet arrays with an average thickness of about 40 nm are uniformly distributed on the CC substrate. After reacting with Na_2S solution, the original smooth surfaces of the $Ni(OH)_2$ nanosheets become rough (Figure 1b), indicating that part of precursor $Ni(OH)_2$ is sulfurized into NiS. Moreover, the morphology of NiS/$Ni(OH)_2$ nanosheets

shows further changes after the phosphorization process (Figure 1c). The average thickness of nanosheets (about 100 nm) is larger than that of $Ni(OH)_2$ precursor and the material surface becomes more rough. EDX analysis confirmed the distribution of Ni, S, P, O and C elements in the NiS/Ni_2P/CC (Figure S1), and the existence of O element is owing to surface oxidation during exposure in air.[34] Besides, the C signal in the survey scan is quite weak, which may be caused by the excessive amount of catalyst supported on the carbon cloth substrate. The HRTEM were further performed to characterize surface structures and interfaces between NiS and Ni_2P. The HRTEM characterization in Figure 1d reveals that there obviously exists plenty of boundaries for NiS/Ni_2P. The existence of the interface suggests possible electronic interactions between NiS and Ni_2P in the hybrid material and an increase of active sites, which will be further discussed in the following analysis. The two-dimensional lattices (both lattice distances and the angle between two crystallographic directions) of NiS and Ni_2P in different area were presented in the Figure S2a-2d. The interplanar spacings of 0.294 nm and 0.277 nm correspond to the (101) and (300) planes of NiS, respectively (Figure S2b). Besides, the interplanar spacings of 0.281 nm and 0.253 nm correspond to the (101) and (200) planes of Ni_2P, respectively (Figure S2d). Additionally, the Ni, S, and P elements are distributed throughout NiS/Ni_2P nanosheet through STEM EDX mapping analysis (Figure S3a-3e). The corresponding selected area electronic diffraction pattern in Figure S3f confirms that the material is polycrystalline.

XRD characterization was employed to identify the phases and crystallinity of as-prepared materials. Figure 2a shows that $Ni(OH)_2$ was synthesized after hydrothermal process (black curve) (JCPDS no.74-2075). The characteristic peaks of NiS (JCPDS no.86-2280) can be found after the sulfurization treatment (blue curve), indicating that part of the $Ni(OH)_2$ precursor has been sulfurized to form NiS. Additionally, $Ni(OH)_2$ without sulfurization was further converted into

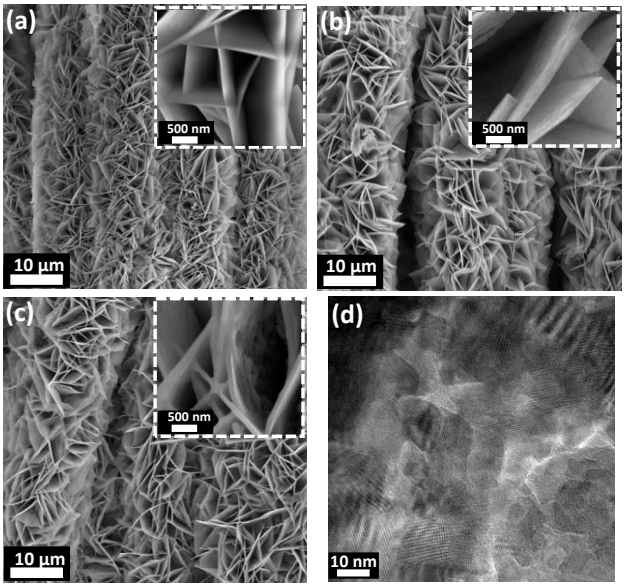

Figure 1. SEM images of (a) $Ni(OH)_2$/CC, (b) NiS/$Ni(OH)_2$/CC, and (c) NiS/Ni_2P/CC; (d) HRTEM image of NiS/Ni_2P/CC.

Ni_2P after the phosphorization treatment (red curve) (JCPDS no. 74-1385), suggesting that the final product is the mixture of NiS and Ni_2P. For comparisons, pure NiS and Ni_2P nanosheet arrays were separately grown on carbon cloth (denoted as NiS/CC and Ni_2P/CC, respectively), and the results of XRD analysis are shown in Figure S4a and 4b. All the observed characteristic peaks in XRD pattern can be indexed to pure NiS and Ni_2P phases, respectively. Furthermore, XPS characterization was employed to study the elements chemical states information for NiS/Ni_2P/CC, along with NiS/CC and Ni_2P/CC. Figure 2b shows the corresponding high-resolution Ni spectra. The characteristic peaks at the binding energies (BEs) of 857.3 eV and 875.1 eV can be ascribed to Ni $2p_{3/2}$ and Ni $2p_{1/2}$ in NiS.[35] While the peaks located at about 856.5 eV and 874.3 eV can be ascribed to Ni $2p_{3/2}$ and Ni $2p_{1/2}$ in Ni_2P.[36] In contrast, the BEs of Ni $2p_{3/2}$ (856.8 eV) and Ni $2p_{1/2}$ (874.4 eV) in NiS/Ni_2P show a negative shift compared with NiS, and a positive shift compared with Ni_2P. Similarly, the BEs for S $2p_{3/2}$ and S $2p_{1/2}$ in NiS/Ni_2P exhibit a negative shift compared to pure NiS (Figure 2c), and the BEs of P 2p in NiS/Ni_2P show a positive shift compared to Ni_2P

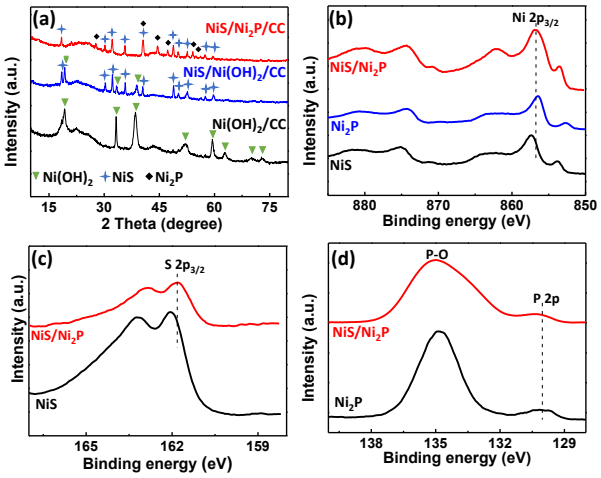

Figure 2. (a) XRD patterns of $Ni(OH)_2$/CC, NiS/$Ni(OH)_2$/CC, and NiS/Ni_2P/CC; high-resolution XPS of (b) Ni 2p, (c) S 2p, and (d) P 2p of the as-prepared catalysts.

(Figure 2d). The shift of binding energy caused by the interfacial charge redistribution between NiS and Ni_2P suggests a change in the electronic structure of NiS/Ni_2P/CC. Small difference in electronic structure of catalyst could lead significant change in chemical properties.[37] Therefore, the charge redistribution in the NiS/Ni_2P/CC hybrid would be another crucial role for the improved catalytic activity.

To assess the catalytic activities of NiS/Ni_2P/CC electrode toward HER (Figure 3a) and OER (Figure 3c), the polarization curves were carried out in 1 M KOH solution. For comparisons, electrocatalytic activities of NiS/CC, Ni_2P/CC, bare CC, RuO_2, and Pt/C were also investigated. As shown in Figure 3a, the NiS/Ni_2P/CC requires a HER overpotential of 111 mV to generate 20 mA cm^{-2}, being lower than that of NiS/CC (158 mV) or Ni_2P/CC (126 mV). Besides, the NiS/Ni_2P/CC electrode shows better HER activity at high current densities, e.g 300 mA cm^{-2}, which approaches the catalytic activity of the benchmark Pt/C electrode at same current density. The control experiment using the bare CC electrode shows negligible catalytic activity for HER. Meanwhile, the LSV polarization curves of the as-prepared catalysts for HER without iR-corrected were shown in Figure S5a. Additionally, considering the difference in mass loading of the as-

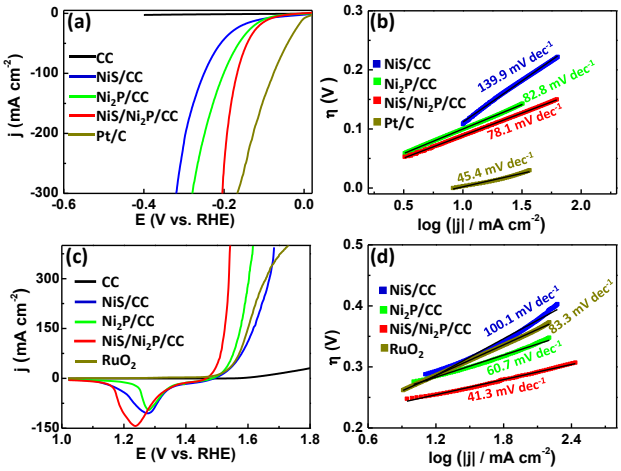

Figure 3. (a) and (b) the iR-corrected LSV curves and the Tafel plots of various catalysts for HER; (c) and (d) the iR-corrected LSV curves and the Tafel plots of various catalysts for OER.

prepared catalysts, we further compared the mass activity per unit area of all the catalysts. As shown in Figure S6a, NiS/Ni_2P/CC still exhibits the best mass activity for HER among the compared samples. To better understand HER mechanism, the Tafel slopes are determined from the equation of $\eta = b \log (j) + a$. The Tafel slope for NiS/Ni_2P/CC electrode is 76.1 mV dec^{-1} (Figure 3b), which is smaller than NiS/CC electrode (139.9 mV dec^{-1}) and Ni_2P/CC electrode (82.8 mV dec^{-1}), indicating faster kinetics and higher hydrogen generation rate during the process of HER.[38] According to the established mechanisms for HER in alkaline media, when the Tafel slope is *ca*. 120 mV dec^{-1}, the Volmer reaction ($H_2O + e^- \rightarrow H_{ads} + OH^-$) is the rate-determining step, and when the Tafel slope is *ca*. 40 or 30 mV dec^{-1}, the Heyrovsky reaction ($H_{ads} + e^- + H_2O \rightarrow OH^- + H_2$) or the Tafel reaction ($H_{ads} + H_{ads} \rightarrow H_2$) is the rate-determining step.[39] The Tafel slope for the NiS/Ni_2P/CC electrode lies in the range of 40 to 120 mV dec^{-1}, implying NiS/Ni_2P/CC electrode proceeds *via* the Volmer-Heyrovsky mechanism and the electrochemical recombination is the rate-determining step during the process of HER.[40] Additionally, the exchange current density (j_0) for NiS/Ni_2P/CC electrode was calculated to be about 0.68 mA cm^{-2}, being higher than the other Pt-free electrocatalysts such as MoP NPs (0.046 mA cm^{-2}),[41] Ni-Mo-N (0.67 mA cm^{-2}),[42]

and FeB_2 (0.245 mA cm^{-2}),[43] indicating a higher intrinsic electron transfer rate at the interface of NiS/Ni_2P/CC electrode and alkaline electrolyte.

Figure 3c shows the iR-corrected LSV curves of as-obtained materials toward OER. The current "shoulder" at about 1.4 V vs. RHE can be attributed to anodic oxidation of Ni-based species. Besides, the strong signal intensity of the oxidation peak of Ni species may be related to the amount of catalyst loading and the exposed Ni-based active sites. Similarly phenomenon on Ni-based phosphides have been reported by Sun's group and Liu's group.[44,45] Furthermore, the polarization curve of pure $Ni(OH)_2$/CC electrode exhibits a quite weak oxidation peak at about 1.4 V (Figure S7), indicating that the strong oxidation peak for NiS/Ni_2P/CC is probably not caused by the incomplete conversion of $Ni(OH)_2$ during the sulfurization or phosphorization process. Meanwhile, cyclic voltammogram (CV) of as-prepared samples were shown in Figure S8a-8c. Since there is a significant oxidation peak of the Ni species prior to the OER process in the forward scan, the required OER overpotentials to generate 20 mA cm^{-2} are determined from the reverse scan LSV curves. A small OER overpotential of 265 mV is obtained for the NiS/Ni_2P/CC electrode at 20 mA cm^{-2} (Figure 3c), which is superior to the benchmark RuO_2 electrode (291 mV) and outperforms other reported OER catalysts at the same current density, such as NiS (η = 335 mV)[46] and Ni-P (η = 320 mV).[47] Besides, NiS/Ni_2P/CC electrode shows a higher activity than NiS/CC (292 mV) and Ni_2P/CC (308 mV) at the same current density. Meanwhile, the LSV polarization curves of the as-prepared catalysts for OER without iR-corrected were shown in Figure S5b. Furthermore, NiS/Ni_2P/CC still exhibits the best mass activity for OER among the compared samples (Figure S6b). The Tafel plots for OER were further determined from the LSV curves, which are swept from positive to negative (Figure 3d). The NiS/Ni_2P/CC electrode exhibits the relatively small Tafel slope of 41.3 mV dec^{-1} among all catalyst materials investigated in this study, including

RuO_2 (83.3 mV dec^{-1}), NiS/CC (100.1 mV dec^{-1}), and Ni_2P/CC (60.7 mV dec^{-1}), suggesting favorable kinetics for OER on NiS/Ni_2P/CC electrode. Meanwhile, the calculated j_0 for NiS/Ni_2P/CC electrode is about 2.5×10^{-4} mA cm^{-2}, being higher than other OER catalyst such as Co_3O_4 (6.0×10^{-6} mA cm^{-2}).[48]

We measured the double layer capacitance (C_{dl}) in a non-Faradaic potential region to assess electrochemically active surface area (ECSA) of catalysts (Figure S9a-9c).[25] The obtained ECSA value for the NiS/Ni_2P/CC (480 cm^2) is significantly larger than that of NiS/CC (128 cm^2) and Ni_2P/CC (172 cm^2). This implies that the abundant the phase boundaries between NiS and Ni_2P in the composite could create more exposed active sites and thus contribute to an enhanced ECSA for the NiS/Ni_2P/CC. The improved ECSA for NiS/Ni_2P/CC electrode is beneficial to the enhanced anion exchangeability between electrolytes and catalytic active sites, which definitely contributes to the significantly improved catalytic performance. The turnover frequency (TOF) was calculated to investigate the intrinsic activity of the materials for HER and OER.[49] The detailed calculation method was shown in the supporting information The TOF of NiS/Ni_2P/CC electrode for HER is calculated to be 0.901 s^{-1} at an overpotential of 200 mV, being higher than that of NiS/CC (0.603 s^{-1}) and Ni_2P/CC (0.857 s^{-1}). Meanwhile, the TOF of NiS/Ni_2P/CC for OER is estimated to be 0.331 s^{-1} at an overpotential of 300 mV, which is higher than that of NiS/CC (0.142 s^{-1}) and Ni_2P/CC (0.146 s^{-1}). These results indicate a higher intrinsic HER and OER activity on NiS/Ni_2P/CC than that on NiS/CC and Ni_2P/CC. Moreover, we carried out the electrochemical impedance spectroscopy (EIS) measurement to evaluate the charge transfer resistance of as-obtained materials.[50,51] As shown in Figure 4b, The Nyquist plots of as-obtained catalysts at -0.25 V show an apparent semicircle in lower frequency region, which is associated with charge transfer

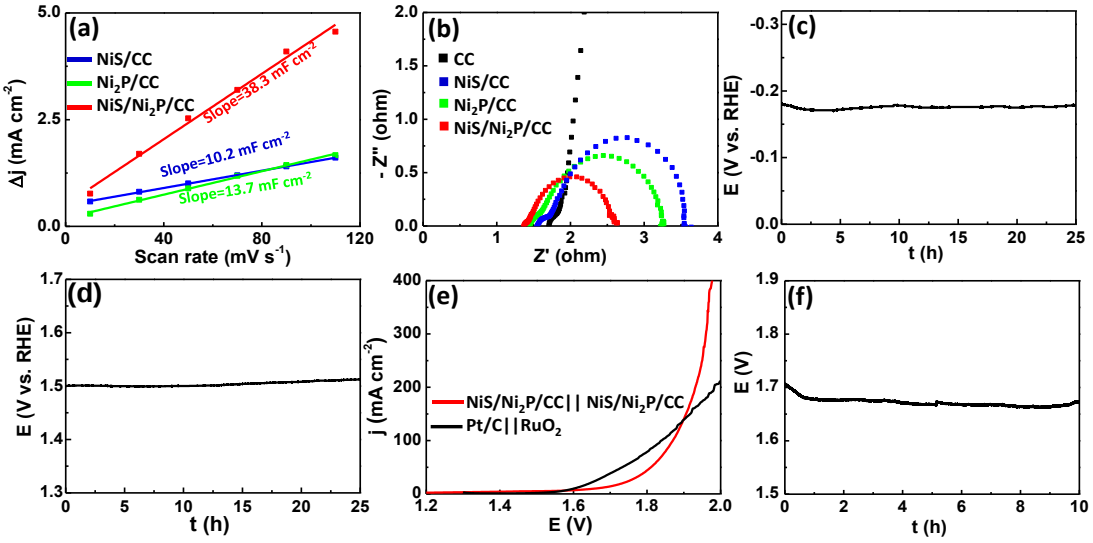

Figure 4. (a) ΔJ (Ja-Jc) of various catalysts plotted against the scanning rates; (b) Nyquist plots of various catalysts at -0.25 V; (c) and (d) chronopotentiometry measurements of NiS/Ni_2P/CC for HER and OER at an current density of 20 mA cm^{-2}; (e) LSV polarization curves of two-electrode water splitting system for the NiS/Ni_2P/CC||NiS/Ni_2P/CC and Pt/C||RuO_2; (f) chronopotentiometry measurement of the NiS/Ni_2P/CC||NiS/Ni_2P/CC electrolyzer at an current density of 10 mA cm^{-2}.

resistance (R_{ct}). Smaller value of R_{ct} represents faster electrochemical reaction rate. The smaller R_{ct} for NiS/Ni_2P/CC electrode comparing to NiS/CC and Ni_2P/CC indicates the faster charge transport among all the studied counterparts. This result is consistent with the lower Tafel slope for NiS/Ni_2P/CC electrode in Figure 4b and 4d. In short, the strong electronic interactions between NiS and Ni_2P, the enhanced catalytically active sites, and the faster charge transport kinetics contribute to the superior electrocatalytic activity for both HER and OER on NiS/Ni_2P/CC electrode comparing to NiS/CC and Ni_2P/CC.

Long-term stability under harsh HER and OER conditions is another critical issue for the application of a promising electrocatalyst. Therefore, the stability of the NiS/Ni_2P/CC electrode for HER and OER were measured in alkaline solution using chronopotentimetry at 20 mA cm^{-2}. The NiS/Ni_2P/CC electrode shows a stable potential response for both HER and OER and without

significant degradation after 25 hrs of continuous electrolysis (Figure 4cand 4d). SEM images of NiS/Ni_2P/CC after long term HER and OER stability tests (Figure S10a and 10b) exhibit no apparent change in morphology, further confirming the good stability of the NiS/Ni_2P/CC. Besides, XPS characterization was further conducted to analyze the change of surface structure of NiS/Ni_2P/CC electrode after stability tests. As shown Figure S11a-11c, the characteristic peaks of Ni 2p (at about 853.2 eV), P 2p (at about 129.9 eV), and S 2p (at ca. 162 eV) corresponding to Ni-P and Ni-S bonding in NiS/Ni_2P/CC still exist after HER stability test. The relatively low peak could directly be attributed to the formation of phosphate on the surface [52]. Besides, these characteristic peaks mentioned above have completely disappeared after OER stability test. The remaining peak at about 856 eV for Ni 2p can be attributed to the formed Ni hydroxides species during the OER process according to reported studies [53-55]. Meanwhile, the elemental analysis from the EDX shows that the content of O in NiS/Ni_2P/CC after stability tests is significantly high than the newly prepared sample (Table S1), which further confirmed an oxidation on the surface of NiS/Ni_2P/CC during the process of HER and OER. Furthermore, the HRTEM in Figure S12a and 12b confirmed that the amorphous shell was formed on the surface of the NiS/Ni_2P/CC.

Based on the bifunctional property of the material, NiS/Ni_2P/CC was applied as both anode and cathode in the overall water splitting electrolyzer. The assembled electrolyzer requires a 1.67 V cell voltage to reach 10 mA cm^{-2} (Figure 4e). This performance is even comparable to the assembled electrolyzer using nickel-based catalysts such as Ni_xP_y (1.58 V) and Ni_2P (1.63 V) at the same current density.[52,56] Furthermore, the performance of NiS/Ni_2P/CC||NiS/Ni_2P/CC electrolyzer outperforms precious metal catalysts at high current densities. For instance, the NiS/Ni_2P/CC||NiS/Ni_2P/CC electrolyzer needs 1.87 V voltage to achieve 200 mA cm^{-2}, which is lower than that of the Pt/C||RuO_2 electrolyzer (1.98 V). In addition, the electrocatalytic

performance of the NiS/Ni_2P/CC electrode is better than most of other reported bifunctional catalysts for water splitting (Table S2). Finally, the NiS/Ni_2P/CC||NiS/Ni_2P/CC electrolyzer maintains an excellent stability for over 10 hrs bulk water electrolysis (Figure 4f), which laid a solid foundation for the long-term application of the electrolysis.

4. CONCLUSION

In summary, a strategy to enhance electrocatalytic activity of water splitting by forming a hybrid structure has been demonstrated. The as-obtained NiS/Ni_2P/CC catalyst shows excellent electrochemical activity and superior long-term durability for both HER and OER. The outstanding electrochemical activity of NiS/Ni_2P/CC is attributed to strong electronic interactions between NiS and Ni_2P, abundant active sites, and enhanced smaller charge transfer resistance. The NiS/Ni_2P electrocatalyst grown directly on the conductive substrate without complicated pre- or post-treatments is robust and reliable for long-term water splitting. Furthermore, the material design presented in this study can also be extended to fabricate other non-noble metal catalysts for the application in electrochemical energy conversion and storage.

ASSOCIATED CONTENT

Supporting Information. Additional information are available mentioned in the text, which includes EDX spectrum, the elemental mapping images, and the HRTEM image of NiS/Ni_2P/CC; XRD patterns of samples for NiS/CC and Ni_2P/CC; the CV curves of as-obtained catalysts; without iR-corrected LSV curves for OER and HER; typical CV curves of electrode NiS/CC, Ni_2P/CC and NiS/Ni_2P/CC in with different scanning rates; SEM images, XPS analysis, and elements analysis (Table S1) of NiS/Ni_2P/CC after HER and OER stability test; comparison of electrochemical performance for NiS/Ni_2P/CC with other bifunctional electrocatalysts (Table S2).

AUTHOR INFORMATION

Corresponding Author

*E-mail: ciac_sheny@mail.hust.edu.cn.

Notes

The authors declare no competing financial interest.

ACKNOWLEDGEMENTS

This work was financially supported from the 973 Program of China (2014CB643506), the NSFC Major International (Regional) Joint Research Project NSFC-SNSF (51661135023), NSFC (21673091), the Fundamental Research Funds for the Central Universities (HUST: 2016YXMS031), the Director Fund of the WNLO, and the Open Funds of the State Key Laboratory of Electroanalytical Chemistry (SKLEAC201607) and an Australian Research Council Discovery project (DP160103107). The authors thank the Analytical and Testing Center of HUST and the Center of Micro-Fabrication and Characterization of WNLO for the measurements.

REFERENCES

(1) Zou, X. X.; Zhang, Y. Noble Metal-free Hydrogen Evolution Catalysts for Water Splitting. *Chem. Soc. Rev*. **2015**, *44*, 5148-5180.

(2) Turner, J. A. A Realizable Renewable Energy Future. *Science*, **1999**, *285*, 687-689.

(3) De Souzaa, R. F.; Padilhaa, J. C.; Gonçalvesa, R. S.; de Souzaa, M. O.; Rault-Berthelotb, J. Electrochemical Hydrogen Production from Water Electrolysis Using Ionic Liquid as Electrolytes: Towards the Best Device. *J. Power Sources* **2007**, *164*, 792-798.

(4) Lin, H. L.; Liu, N.; Shi, Z. P.; Guo, Y. L.; Tang, Y.; Gao, Q. S. Cobalt-doping in Molybdenum Carbide Nanowires Toward Efficient Electrocatalytic Hydrogen Evolution. *Adv. Funct. Mater*. **2016**, *26*, 5590-5598.

(5) Liu, W.; Hu, E. Y.; Jiang, H.; Xiang, Y. J.; Weng, Z.; Li, M.; Fan, Q.; Yu, X. Q.; Altman, E.; Wang, H. L. A Highly Active and Stable Hydrogen Evolution Catalyst Based on Pyrite-Structured Cobalt Phosphosulfide. *Nat. Commun*. **2016**, *7*, 10771.

(6) McCrory, C. C. L.; Jung, S.; Peters, J. C.; Jaramillo, T. F. Benchmarking Heterogeneous Electrocatalysts for the Oxygen Evolution Reaction. *J. Am. Chem. Soc*. **2013**, *135*, 16977-16987.

(7) Kanan, M. W.; Nocera, D. G. In Situ Formation of an Oxygen-Evolving Catalyst in Neutral Water Containing Phosphate and Co^{2+}. *Science* **2008**, *321*, 1072-1075.

(8) Zhang, Y. Q.; Ouyang, B.; Xu, J.; Chen, S.; Rawat, R. S.; Fan, H. J. 3D Porous Hierarchical Nickel-Molybdenum Nitrides Synthesized by RF Plasma as Highly Active and Stable Hydrogen-Evolution-Reaction Electrocatalysts. *Adv. Energy Mater*. **2016**, *6*, 1600221.

(9) Xing, Z. C.; Li, Q.; Wang, D. W.; Yang, X. R.; Sun, X. P. Self-Supported Nickel Nitride as an Efficient High-Performance Three-Dimensional Cathode for the Alkaline Hydrogen Evolution Reaction. *Electrochimica Acta* **2016**, *191*, 841-845.

(10) Li, J. S.; Wang, Y.; Liu, C. H.; Li, S. L.; Wang, Y. G.; Dong, L. Z.; Dai, Z. H.; Li, Y. F.; Lan, Y. Q. Coupled Molybdenum Carbide and Reduced Graphene Oxide Electrocatalysts for Efficient Hydrogen Evolution. *Nat. Commun*. **2016**, *7*, 11204.

(11) Huang, Y.; Gong, Q. F.; Song, X. N.; Feng, K.; Nie, K. Q.; Zhao, F. P.; Wang, Y. Y.; Zeng, M.; Zhong, J.; Li, Y. G. Mo_2C Nanoparticles Dispersed on Hierarchical Carbon Microflowers for Efficient Electrocatalytic Hydrogen Evolution. *ACS Nano* **2016**, *10*, 11337-11343.

(12) Wu, Z. X.; Wang, J.; Xia, K. D.; Lei, W.; Liu, X. E.; Wang, D. L. MoS_2-MoP Heterostructured Nanosheets on Polymer-derived Carbon as an Electrocatalyst for Hydrogen Evolution Reaction. *J. Mater. Chem. A*, **2018**, *6*, 616-622.

(13) Grimaud, A.; May, K. J.; Carlton, C. E.; Lee, Y. L.; Risch, M.; Hong, W. T.; Zhou, J. G.; Shao-Horn, Y. Double Perovskites as a Family of Highly Active Catalysts for Oxygen Evolution in Alkaline Solution. *Nat. Commun*. **2013**, *4*, 2439.

(14) Suntivich, J.; May, K. J.; Gasteiger, H. A.; Goodenough, J. B. Shao-Horn, Y. A Perovskite Oxide Optimized for Oxygen Evolution Catalysis from Molecular Orbital Principles. *Science* **2011**, *334*, 1383-1385.

(15) Zhang, G. X.; Yang, J.; Wang, H.; Chen, H. B.; Yang, J. L.; Pan, F. $Co_3O_{4-\delta}$ Quantum Dots as a Highly Efficient Oxygen Evolution Reaction Catalyst for Water Splitting. *ACS Appl. Mater. Interfaces* **2017**, *9*, 16159-16167.

(16) Seitz, L. C.; Nordlund, D.; Gallo, A.; Jaramillo, T. F. Tuning Composition and Activity of Cobalt Titanium Oxide Catalysts for the Oxygen Evolution Reaction. *Electrochimica Acta* **2016**, *193*, 240-245.

(17) Liang, H. F.; Meng, F.; Caban-Acevedo, M.; Li, L. S.; Forticaux, A.; Xiu, L. C.; Wang, Z. C.; Jin, S. Hydrothermal Continuous Flow Synthesis and Exfoliation of NiCo Layered Double Hydroxide Nanosheets for Enhanced Oxygen Evolution Catalysis. *Nano Lett*. **2015**, *15*, 1421-1427.

(18) Lu, X.; Zhao, C. Electrodeposition of Hierarchically Structured Three-Dimensional Nickel-Iron Electrodes for Efficient Oxygen Evolution at High Current Densities. *Nat. Commun*. **2015**, *6*, 6616.

(19) Wang, X. G.; Li, W.; Xiong, D. H.; Petrovykh, D. Y.; Liu, L. F. Bifunctional Nickel Phosphide Nanocatalysts Supported on Carbon Fiber Paper for Highly Efficient and Stable Overall Water Splitting. *Adv. Funct. Mater*. **2016**, *26*, 4067-4077.

(20) Wu, Y. Y.; Li, G. D.; Liu, Y. P. Yang, L.; Lian, X. R.; Asefa, T.; Zou, X. X. Overall Water Splitting Catalyzed Efficiently by an Ultrathin Nanosheet-Built Hollow Ni_3S_2-Based Electrocatalyst. *Adv. Funct. Mater*. **2016**, *26*, 4839-4847.

(21) Kuang, M.; Zheng, G. F.; Nanostructured Bifunctional Redox Electrocatalysts. *Small* **2016**, *12*, 5656-5675.

(22) Li, J. Y.; Li, J.; Zhou, X. M.; Xia, Z. M.; Gao, W.; Ma, Y. Y.; Qu, Y. Q. Highly Efficient and Robust Nickel Phosphides as Bifunctional Electrocatalysts for Overall Water-Splitting. *ACS Appl. Mater. Interfaces* **2016**, *8*, 10826-10834.

(23) Zhang, J.; Wang, T.; Pohl, D.; Rellinghaus, B.; Dong, R. H.; Liu, S. H.; Zhuang, X. D.; Feng, X. L. Interface Engineering of MoS_2/Ni_3S_2 Heterostructures for Highly Enhanced Electrochemical Overall-Water-Splitting Activity. *Angew. Chem. Int. Ed.* **2016**, *128*, 6814-6819.

(24) Zhang, H. C.; Li, Y. J.; Xu, T. H.; Wang, J. B.; Huo, Z. Y.; Wan, P. B.; Sun, X. M. Amorphous Co-doped MoS_2 Nanosheet Coated Metallic CoS_2 Nanocubes as an Excellent Electrocatalyst for Hydrogen Evolution. *J. Mater. Chem. A* **2015**, *3*, 15020-15023.

(25) Tran, P. D.; S. Y. Chiam, P. P. Boix, Ren, Y.; Pramana, S. S.; Fize, J.; Artero, V.; Barber, J. Novel Cobalt/Nickel-Tungsten-Sulfide Catalysts for Electrocatalytic Hydrogen Generation from Water. *Energy Environ. Sci*. **2013**, *6*, 2452-2459.

(26) Long, X.; Li, G. X.; Wang, Z. L.; Zhu, H. Y.; Zhang, T.; Xiao, S.; Guo, W. Y.; Yang, S. H. Metallic Iron-Nickel Sulfide Ultrathin Nanosheets as a Highly Active Electrocatalyst for Hydrogen Evolution Reaction in Acidic Media. *J. Am. Chem. Soc*. **2015**, *137*, 11900-11903.

(27) Sun, J. M.; Chen, Y. J.; Ren, Z. Y.; Fu, H. Y.; Xiao, Y. T.; Wang, J. G.; Tian, G. H. Self-Supported NiS Nanoparticle-Coupled Ni_2P Nanoflake Array Architecture: An Advanced Catalyst for Electrochemical Hydrogen Evolution. ChemElectroChem **2017**, *4*, 1-9.

(28) Du, C. C.; Shang, M. X.; Mao, J. X.; Song, W. B. Hierarchical MoP/Ni_2P Heterostructures on Nickel Foam for Efficient Water Splitting. *J. Mater. Chem. A* **2017**, 5, 15940-15949.

(29) An, T.; Wang, Y.; Tang, J.; Wei, W.; Cui, X. Q.; Alenizi, A. M.; Zhang, L. J.; Zheng, G. F. Interlaced NiS_2-MoS_2 Nanoflake-Nanowires as Efficient Hydrogen Evolution Electrocatalysts in Basic Solutions. *J. Mater. Chem. A* **2016**, *4*, 13439-13443.

(30) Wang, F. M.; He, P.; Li, Y. C.; Shifa, T. A.; Deng, Y.; Liu, K. L.; Wang, Q. S.; Wang, F.; Wen, Y.; Wang, Z. X.; Zhan, X. Y.; Sun, L. F.; He, J. Interface Engineered W_xC@WS_2 Nanostructure for Enhanced Hydrogen Evolution Catalysis. *Adv. Funct. Mater*. **2017**, *27*, 1605802.

(31) Li, J.; Guo, L. T.; Shangguan, E. B.; Yue, M. Z; Xu, M.; Wang, D.; Chang, Z. R.; Li. Q. M. Synthesis of Novel Spherical Fe_3O_4@Ni_3S_2 Composite As Improved Anode Material for Rechargeable Nickel-Iron Batteries. *Electrochimica Acta* **2017**, *240*, 456-465.

(32) Xiao, X.; Huang, D. K.; Luo, Y. P.; Li, M.; Wang, M. K.; Shen, Y. Ultrafine Pt Nanoparticle Decoration with CoP as Highly Active Electrocatalyst for Alcohol Oxidation. *RSC Adv*. **2016**, *6*, 100437-100442.

(33) Tang, C.; Cheng, N. Y.; Pu, Z. H.; Xing, W.; Sun, X. P. NiSe Nanowire Film Supported on Nickel Foam: an Efficient and Stable 3D Bifunctional Electrode for Full Water Splitting. *Angew. Chem. Int. Ed*. **2015**, *54*, 9351-9355.

(34) Jiang, P.; Liu, Q.; Ge, C. J.; Cui, W.; Pu, Z. H.; Asiri, A. M.; Sun, X. P. CoP Nanostructures with Different Morphologies: Synthesis, Characterization and a Study of Their Electrocatalytic Performance toward the Hydrogen Evolution Reaction. *J. Mater. Chem. A* **2014**, *2*, 14634-14640.

(35) Sun, C. C.; Ma, M. Z.; Yang, J.; Zhang, Y. F.; Chen, P.; Huang, W.; Dong, X. C. Phase-Controlled Synthesis of α-NiS Nanoparticles Confined in Carbon Nanorods for High Performance Supercapacitors. *Sci. Rep*. **2014**, *4*, 7054.

(36) Liang, X.; Zheng, B. X.; Chen, L. G.; Zhang, J. T.; Zhuang, Z. B.; Chen, B. H. MOF-Derived Formation of Ni_2P-CoP Bimetallic Phosphides with Strong Interfacial Effect toward Electrocatalytic Water Splitting. *ACS Appl. Mater. Interfaces* **2017**, *9*, 23222-23229.

(37) Zhu, H.; Zhang, J. F.; Yanzhang, R. P.; Du, M. L.; Wang, Q. F.; Gao, G. H.; Wu, J. D.; Wu, G. M.; Zhang, M.; Liu, B.; Yao, J. M.; Zhang, X. M. When Cubic Cobalt Sulfide Meets Layered Molybdenum Disulfide: a Core-Shell System toward Synergetic Electrocatalytic Water Splitting. *Adv. Mater*. **2015**, *27*, 4752-4759.

(38) Wang, X. D.; Xu, Y. F.; Rao, H. S.; Xu, W. J.; Chen, H. Y.; Zhang, W. X.; Kuang, D. B.; Su, C. Y. Novel Porous Molybdenum Tungsten Phosphide Hybrid Nanosheets on Carbon Cloth for Efficient Hydrogen Evolution. *Energy Environ. Sci*. **2016**, *9*, 1468-1475.

(39) Luo, Y. P.; Huang, D. K.; Li, M.; Xiao. X.; Shi, W. N.; Wang, M. K.; Su, J.; Shen, Y. MoS_2 Nanosheet Decorated with Trace Loads of Pt as Highly Active Electrocatalyst for Hydrogen Evolution Reaction. *Electrochimica Acta* **2016**, *219*, 187-193.

(40) Wang, T. T.; Wu, L. Q.; Xu, X. B.; Sun, Y.; Wang, Y. Q.; Zhong, W.; Du. Y. W. An Efficient Co_3S_4/CoP Hybrid Catalyst for Electrocatalytic Hydrogen Evolution. *Sci. Rep.* **2017**, *7*, 11891.

(41) Chen, X. B.; Wang, D. Z.; Wang, Z. P.; Zhou, P.; Wu, Z. Z.; Jiang, F. Molybdenum Phosphide: A New Highly Efficient Catalyst for the Electrochemical Hydrogen Evolution Reaction. *Chem. Commun.* **2014**, *50*, 11683-11685.

(42) Wang, T.; Wang, X.; Liu, Y.; Zheng, J.; Li, X. A Highly Efficient and Stable Biphasic Nanocrystalline Ni-Mo-N Catalyst for Hydrogen Evolution in Both Acidic and Alkaline Electrolytes. *Nano Energy* **2016**, *22*, 111-119.

(43) Li, H.; Wen, P.; Li, Q.; Dun, C. C.; Xing, J. H.; Lu, C.; Adhikari, S. B.; Jiang, L.; Carroll, D. L.; Geyer, S. M. Earth-Abundant Iron Diboride (FeB_2) Nanoparticles as Highly Active Bifunctional Electrocatalysts for Overall Water Splitting. *Adv. Energy Mater*. **2017**, *7*, 1700513.

(44) You, B.; Jiang, N.; Sheng, M. L.; Bhushan, M. W.; Sun, Y. J. Hierarchically Porous Urchin-Like Ni_2P Superstructures Supported on Nickel Foam as Efficient Bifunctional Electrocatalysts for Overall Water Splitting. *ACS Catal*. **2016**, *6*, 714-721.

(45) Wang, X. G.; Li, W.; Xiong, D. H.; Liu, L. F. Fast Fabrication of Self-Supported Porous Nickel Phosphide Foam for Efficient, Durable Oxygen Evolution and Overall Water Splitting. *J. Mater. Chem. A* **2016**, *4*, 5639-5646.

(46) Zhu, W. X.; Yue, X. Y.; Zhang, W. T.; Yu, S. X.; Zhang, Y. H.; Wang, J.; Wang, J. L. Nickel Sulfide Microsphere Film on Ni Foam as an Efficient Bifunctional Electrocatalyst for Overall Water Splitting. *Chem. Commun*. **2016**, *52*, 1486-1489.

(47) Yu, X. Y.; Feng, Y.; Guan, B. Y.; Lou, X. W.; Paik, U. Carbon Coated Porous Nickel Phosphides Nanoplates for Highly Efficient Oxygen Evolution Reaction. *Energy Environ. Sci.* **2016**, *9*, 1246-1250.

(48) Liu, Y. C.; Koza, J. A.; Switzer, J. A. Conversion of Electrodeposited $Co(OH)_2$ to CoOOH and Co_3O_4, and Comparison of Their Catalytic Activity for the Oxygen Evolution Reaction. *Electrochimica Acta* **2014**, *140*, 359-365.

(49) Zhang, R.; Wang, X. X.; Yu, S. J.; Wen, T.; Zhu, X. W.; Yang, F. X; Sun, X. N.; Wang, X. K.; Hu W. P. Ternary $NiCo_2P_x$ Nanowires as pH-Universal Electrocatalysts for Highly Efficient Hydrogen Evolution Reaction. *Adv. Mater*. **2017**, *29*, 1605502.

(50) Song, F.; Hu, X. L. Exfoliation of Layered Double Hydroxides for Enhanced Oxygen Evolution Catalysis. *Nat. Commun*. **2014**, *5*, 4477.

(51) Xiao, X.; Tao, L. M.; Li, M.; Lv, X. W.; Huang, D. K.; Jiang, X. X.; Pan, H. P.; Wang, M. K.; Shen, Y. Electronic Modulation of Transition Metal Phosphide via Doping as Efficient and pH-universal Electrocatalysts for Hydrogen Evolution Reaction. *Chem. Sci.* **2018**, DOI: 10.1039/C7SC04849A.

(52) Menezes, P. W.; Indra, A.; Das, C.; Walter, C.; Göbel, C.; Gutkin, V.; Schmeiβer, D.; Driess, M. Uncovering the Nature of Active Species of Nickel Phosphide Catalysts in High-Performance Electrochemical Overall Water Splitting. *ACS Catal*. **2017**, *7*, 103-109.

(53) Wang, X. G.; Li, W.; Xiong, D. H.; Petrovykh, D. Y.; Liu, L. F. Bifunctional Nickel Phosphide Nanocatalysts Supported on Carbon Fiber Paper for Highly Efficient and Stable Overall Water Splitting. *Adv. Funct. Mater*. **2016**, *26*, 4067-4077.

(54) Wang, M. M.; Lin, M. T.; Li, J. T.; Huang, L.; Zhuang, Z. C.; Lin, C.; Zhou, L.; Mai, L. Q. Metal-Organic Framework Derived Carbon-confined Ni_2P Nanocrystals Supported on Graphene for An Efficient Oxygen Evolution Reaction. *Chem. Commun*. **2017**, *53*, 8372-8375.

(55) Liang, H. F.; Gandi, A. N.; Anjum, D. H.; Wang, X. B.; Schwingenschlögl, U.; Alshareef, H. N. Plasma-Assisted Synthesis of NiCoP for Efficient Overall Water Splitting. *Nano Lett*. **2016**, *16*, 7718-7725.

(56) Stern, L. A.; Feng, L. G.; Song, F.; Hu, X. L. Ni_2P as a Janus Catalyst for Water Splitting: the Oxygen Evolution Activity of Ni_2P Nanoparticles. *Energy Environ. Sci*. **2015**, *8*, 2347-2351.

Table of Contents